BNL-67517

COMPARISON OF COLUMNAR WATER VAPOR MEASUREMENTS DURING THE FALL 1997 ARM INTENSIVE OBSERVATION PERIOD: SOLAR TRANSMITTANCE METHODS

B. Schmid,[1] J. J. Michalsky,[2] D. W. Slater,[3] J. C. Barnard,[3] R. N. Halthore,[4] J. C. Liljegren,[5] B. N. Holben,[6] T. F. Eck,[7] J. M. Livingston,[8] P. B. Russell,[9] T. Ingold,[10] and I. Slutsker[11]

June 2000

Submitted to
Applied Optics

[1] Bay Area Environmental Research Institute, 3430 Noriega Street, San Francisco, CA 94122.
[2] Atmospheric Sciences Research Center, SUNY Albany, 251 Fuller Road, Albany, NY 12203.
[3] Pacific Northwest National Laboratory, P.O. Box 999, Richland, WA 99352.
[4] Brookhaven National Laboratory, P.O. Box 5000, Upton, NY 11973-5000.
[5] Now at: Argonne National Laboratory, 9700 South Cass Ave., Argonne, IL 60439.
[6] NASA Goddard Space Flight Center, Code 923, Greenbelt, MD 20771.
[7] Raytheon ITSS/NASA Goddard Space Flight Center, Code 923, Greenbelt, MD 20771.
[8] SRI International, 333 Ravenswood Avenue, Menlo Park, CA 94025.
[9] NASA Ames Research Center, MS 245-5, Moffett Field, CA 94035-1000.
[10] Institute of Applied Physics, University of Bern, Sidlerstr. 5, CH-3012 Bern, Switzerland.
[11] SSAI/NASA Goddard Space Flight Center, Code 923, Greenbelt, MD 20771.

By acceptance of this article, the publisher and/or recipient acknowledges the U.S. Government's right to retain a nonexclusive, royalty-free license in and to any copyright covering this paper.

Research by BNL investigators was performed under the auspices of the U.S. Department of Energy under Contract No. DE-AC02-98CH10886.

Abstract. In the fall of 1997, during an Intensive Observation Period (IOP), the Atmospheric Radiation Measurement (ARM) program conducted a study of water vapor abundance measurement at its Southern Great Plains (SGP) site. Among a large number of instruments, four sun-tracking radiometers were present to measure the columnar water vapor (CWV). All four solar radiometers retrieve CWV by measuring total solar transmittance in the 0.94-μm water vapor absorption band and subtracting contributions due to Rayleigh, ozone and aerosol transmittances. The aerosol optical depth comparisons among the same four radiometers has been presented elsewhere (*Geophys. Res. Lett.*, 26, 17, 2725-2728, 1999).

We have used three different methods to retrieve CWV. In a first round of comparison no attempt was made to standardize on the same radiative transfer model and its underlying water vapor spectroscopy. In the second round of comparison we used the same line-by-line code (which includes recently corrected H_2O spectroscopy) to retrieve CWV from all four sun-tracking radiometers. This decreased the mean CWV by 8% or 13%. The spread of 8% in the solar radiometer results found when using the same model is an indication of the other-than-model uncertainties involved in determining CWV from solar transmittance measurements with current instrumentation.

OCIS codes: 010.0010, 010.1110, 010.1320, 010.7340

1. Introduction

Solar transmittance methods can provide water vapor abundance from direct or reflected sunlight measurements in spectral channels in and adjacent to water vapor absorption bands. The so-derived water-vapor transmittance has to be translated into columnar water vapor (CWV). Although this relationship is well known qualitatively,[1] it has proven difficult to quantify. Attempts to do so for water-vapor absorption bands in the near-infrared date back to 1912.[2] But

even in the last decade there has been a steady stream of publications on this subject. For example, results from ground-based retrievals of CWV using sunphotometers (SPM) have been reported widely (see Ingold *et al*.[3] and references therein). Recently, Schmid *et al*.[4] reported on CWV retrievals using an airborne sunphotometer. Instruments aboard satellites, such as SAGE II (Stratospheric Aerosol and Gas Experiment) and POAM II and III (Polar Ozone and Aerosol Measurements) use the solar occultation technique (i.e., they act like a SPM by measuring the solar transmittance through the limb of the atmosphere) to retrieve water vapor.[5,6] Finally, CWV is also retrieved from airborne (such us AVIRIS (Airborne Visible Infra Red Imaging Spectrometer)) and spaceborne (such as POLDER (POLarization and Directionality of the Earth's Reflectance) or MODIS (MODerate-resolution Imaging Spectroradiometer)) instruments that measure the solar radiance reflected by the Earth surface.[7,8,9,10]

Recent findings that the H_2O line intensities in the visible and near infrared portion of the widely used HITRAN-96 database[11] were in error[12] and that H_2O lines (especially weak ones) might be missing from the current databases[13,14] have sparked renewed discussion of the accurate conversion of measured water-vapor transmittance into amounts of water vapor.

In the fall of 1997 the Atmospheric Radiation Measurement (ARM) program[15] conducted the 2nd Intensive Observation Period (IOP) to study water vapor at its Southern Great Plains (SGP) site. Among a large number of systems such as radiosondes, microwave radiometers, raman lidars, Global Positioning System receivers, and an infrared spectrometer, four sun-tracking radiometers were present to measure water vapor.[16]

In this paper we focus on the four sun-tracking radiometers that retrieve CWV by measuring solar transmittance in the 0.94-μm water vapor absorption band. The measurements were made between 15 September and 5 October 1997 at the SGP ARM central facility near Lamont,

Oklahoma (36° 36’ N, 97° 22’ W, 316 m above sea level). Dry to very humid conditions, with CWV ranging from 1 to 5 cm, were experienced over the three-week period. As one of the steps in the CWV retrievals the aerosol component must be subtracted from the total transmittance in the 0.94-μm band. The aerosol optical depth (AOD) comparison among the same four radiometers has been presented previously.[17]

Following the philosophy of the just-mentioned AOD-comparison we first made no attempt to standardize on the methods used to derive CWV from the four radiometers. We found that three different methods had been used in conjunction with three different radiative transfer models. In a second round we used the same radiative transfer model (with its underlying spectroscopy corrected according to Giver *et al.*[12]) for all instruments. In this paper we will show the results from both comparisons.

2. Instrumentation

The NASA Ames Research Center deployed its six-channel Ames Airborne Tracking Sunphotometer (AATS-6) at the SGP central facility of ARM for this IOP. This instrument, described by Matsumoto *et al.*,[18] uses an active sun sensor to keep the instrument pointed at the solar disk. The central wavelengths and full widths at half maximum (FWHM) for the filters are given in Table 1. The Si detectors are held at a constant temperature of 45± 0.6 °C. The field-of-view (FOV) of AATS-6 is 4.5°. A measurement sequence was repeated every 12 seconds with all filters scanned nine times then averaged in the first three seconds of the 12-second period.

At the ARM SGP central facility a CIMEL sun/sky photometer measures AOD. This instrument is also part of AERONET, a worldwide network of CIMEL sunphotometers [*Holben et al.*, 1998].[19] The CIMEL CE-318 points to the sun based on an ephemeris calculation and then fine tunes the pointing with an active sun sensor adjustment. Samples consist of triplets of

measurements with each member of the triplet beginning 30 seconds apart and consisting of eight filter measurements completed within eight seconds; the triplets are repeated at every quarter air mass between two to seven air masses and every 15 minutes when the air mass is less than two. The central wavelength and FWHM for each filter are given in Table 1. The field-of-view is 1.2°. The temperature of the instrument is monitored but not controlled.

The multi-filter rotating shadowband radiometer (MFRSR)[20] has a hemispherical field-of-view. A band is positioned to alternately move completely out of the field-of-view and then to block the sun according to a solar hour angle calculation allowing a measurement of the total downward and diffuse downward irradiance. The difference between the two measurements is the direct solar component normal to the receiver, and the direct normal component is calculated by dividing by the cosine of the solar-zenith angle and correcting for the angular response of the quasi-Lambertian detector. Sampling is every 20 seconds. The central wavelength and FWHM for each filter are given in Table 1. The temperature is held at 40°C.

The rotating shadowband spectroradiometer (RSS)[21] has a Lambertian receiver and a shadowing sequence similar to the MFRSR; however, the detector is a 512-element photodiode array that receives its energy input from the focus of a prism spectrograph. Sampling is performed once each minute. The spectral resolution between 350 and 1050 nm diminishes from 0.3 to 8 nm because of the prism dispersive element. The temperature is held at 40°C.

In the following we will refer to all four instruments as sunphotometers (SPM).

3. Methodology

In the derivation of atmospheric transmittance, we distinguish between atmospheric window channels and gaseous-absorption channels. The window channels are located outside of

molecular absorption bands such as O_2 or H_2O bands, and are normally used to determine the aerosol optical depth.

3.1. Aerosol Optical Depth

For atmospheric window channels the SPM output voltage, (λ), obtained when observing the directly transmitted solar irradiance over a small bandpass $\Delta\lambda$ centered at wavelength λ can be described by the Beer-Lambert-Bouguer attenuation law

$$V(\lambda) = V_o(\lambda) R^{-2}\, exp[-m\tau(\lambda)] \tag{1}$$

where $V_o(\lambda)$ is the instrument calibration constant, R is the Earth-Sun distance in astronomical units (AU) at the time of observation, $\tau(\lambda)$ is the spectral optical depth, and m is the relative optical airmass, a function of the solar zenith angle. Taking the logarithm of (1) leads to

$$\ln V(\lambda) = \ln\left[V_o(\lambda) R^{-2}\right] - m\tau(\lambda) \tag{2}$$

If a series of measurements is taken over a range of airmasses m during which the optical depth $\tau(\lambda)$ remained constant, $V_o(\lambda)$ may be determined from the ordinate intercept of a least-squares fit when plotting the left-hand side of (2) versus m. This procedure is commonly known as Langley-plot calibration.

In (1) several attenuators contribute to $\tau(\lambda)$:

$$\tau(\lambda) = \tau_R(\lambda) + \tau_3(\lambda) + \tau_2(\lambda) + \tau_a(\lambda) \tag{3}$$

where the subscripts *R*, 3, 2 and *a* refer to Rayleigh scattering by air molecules, absorption due to O_3 and O2, and attenuation due to aerosol particles, respectively.

A refined Langley technique[22,23,24] - which uses individual airmass expressions for each attenuator in (3) - was used for AATS-6 but not for the other 3 instruments. The window channels of AATS-6 were calibrated by averaging the results of 6 successful morning Langley

plots performed at the Mauna Loa Observatory (MLO) in Hawaii (19° 32’ N, 155° 34’ W, 3397 m above sea level) about two weeks before the IOP.

Calibration of Cimel #27 (the instrument deployed at SGP during the IOP) is based on a transfer of the calibration from Cimel #37, the reference instrument. The intercalibrations were performed at Goddard Space Flight Center in Maryland on 30 August 1997 and 3 November 1997 at midday for a period of 1-2 hours. The reference instrument itself was calibrated using the Langley technique at MLO in May and September 1997.

Calibration of MFRSR and RSS was based on a robust estimate using the 20 nearest successful Langley plots at SGP. One of those 20 nearest successful Langley plots was obtained with data from the morning of 29 September 1997. A Langley plot performed with AATS-6 during that same morning yielded calibration constants that agreed within 0.5% with the Mauna Loa results obtained two weeks before the IOP. This suggests that during this particular morning the atmosphere over SGP was sufficiently stable to yield unbiased Langley plot results to be used in the robust estimate of the calibration constants for MFRSR and RSS.

Once the calibration constants $V_o(\lambda)$ of the window channels are known the aerosol optical depth $\tau_a(\lambda)$ can be determined from (2) - (3). The AODs obtained from each instrument were derived independently of one another. Although the methods to remove Rayleigh, ozone and nitrogen dioxide optical depths may coincide in some instances, there was no attempt at a uniform reduction to aerosol optical depth from total optical depth. Nevertheless, AODs (λ=380-1020 nm) obtained during the IOP by Cimel, MFRSR and RSS agreed with AATS-6 values to within 0.025 (rms). The AODs in atmospheric “windows” adjacent to the 0.94-μm band agreed within 0.015 (rms).[17]

3.2. Columnar Water Vapor

The Beer-Lambert-Bouguer law, monochromatic in its nature, may be applied over small bandpasses $\Delta\lambda$ with negligible error as long as the spectral variation of transmittance inside the bandpass is small. In regions of strong spectral variation of molecular absorption, such as the near-infrared water-vapor absorption bands, (1) may be expressed as[25]

$$V(\lambda) = V_0(\lambda) R^{-2} \exp\left[-m\left(\tau_R(\lambda) + \tau_a(\lambda) + \tau_3(\lambda)\right)\right] T_w\left(\bar{\lambda}\right) \tag{4}$$

(Note that there is no absorption due to NO_2 in the water-vapor absorption channels used here). $T_w\left(\bar{\lambda}\right)$ is the band- and source-weighted water-vapor transmittance

$$T_w\left(\bar{\lambda}\right) = \frac{\int_{\Delta\lambda} E_0(\lambda) S(\lambda) \exp\left[-m\tau_w(\lambda)\right] d\lambda}{\int_{\Delta\lambda} E_0(\lambda) S(\lambda) d\lambda} \tag{5}$$

where $\tau_w(\lambda)$ is the strongly varying water vapor absorption optical depth, $E_0(\lambda)$ is the exoatmospheric solar irradiance, and $S(\lambda)$ is the instrument response. It should be noted that even if $E_0(\lambda)$ and $S(\lambda)$ were effectively constant over $\Delta\lambda$, the strong spectral variation of $\tau_w(\lambda)$ is sufficient to require the band-weighted transmittance $T_w\left(\bar{\lambda}\right)$ in (4). Also, (4) does not follow the Beer-Lambert-Bouguer law, as $T_w\left(\bar{\lambda}\right)$ generally cannot be modeled by an exponential with a negative argument of airmass times a constant band-weighted optical depth. Hence, for channels in strong absorption bands, $V_o(\lambda)$ can no longer be found using the traditional or refined Langley method. In this paper we discuss three different approaches to determine $V_o(\lambda)$ and $T_w\left(\bar{\lambda}\right)$ in order to determine CWV from measurements in the 0.94-μm water vapor absorption band.

Method A: Modified Langley plot technique

If $T_w(\bar{\lambda})$ can be modeled by an exponential with a negative argument proportional to some power of the slant path absorber amount such as

$$T_w(\bar{\lambda}) = \exp\left[-a(mu)^b\right] \tag{6}$$

where u is the columnar water vapor and a and b are constants, then $V_o(\lambda)$ can be determined using a modified Langley plot technique: Substituting (6) into (4), rearranging the terms and taking the logarithm leads to

$$\ln V(\lambda) + m\left[\tau_a(\lambda) + \tau_R(\lambda) + \tau_3(\lambda)\right] = ln\left[V_o(\lambda)R^{-2}\right] - a(mu)^b \tag{7}$$

Modified Langley plots are now constructed by plotting the left-hand side of (7) versus m^b. Therefore, the instantaneous values of the aerosol optical depth $\tau_a(\lambda)$ in the water-vapor absorption channels are needed. These are estimated from the SPM "window" wavelengths using a quadratic fit on a log-log scale of $\tau_a(\lambda)$ versus λ. This requires the $V_o(\lambda)$ values of the "window" channels to be determined *before* constructing modified Langley-plots. It is evident that for the construction of modified Langley plots the columnar water-vapor amount should remain constant, at least for the 1.5 to 2 hour period of Langley data acquisition.

$T_w(\bar{\lambda})$ is typically computed according to (5) over a range of slant path water vapor amounts using a radiative transfer model. The constants a and b in (6) are then found by a curve-fitting procedure.[3,26,27,28] Combining equations (4) and (6) the CWV is

$$u = \frac{1}{m}\left[\frac{1}{a}\left(\ln\frac{V_o(\lambda)R^{-2}}{V(\lambda)} - m\left[\tau_R(\lambda) + \tau_a(\lambda) + \tau_3(\lambda)\right]\right)\right]^{\frac{1}{b}} \tag{8}$$

In this paper we used method A to obtain CWV for AATS-6 and Cimel. For the Cimel instrument the standard AERONET algorithm was used: the same typical filter function ($S(\lambda)$ in (5)) was used for all instruments in the network in conjunction with LOWTRAN 7 computations[29] to determine one set of *a* and *b*. The 940-nm channel of the reference instrument Cimel #37 was calibrated using the modified Langley technique at MLO in May and September 1997. For both calibration periods the $V_o(\lambda)$ values of 4 morning modified Langley plots were averaged. The relative standard deviations in $V_o(\lambda)$ were ~2%.

For AATS-6 we used MODTRAN 3.5 v1.1[29] to determine one set of *a* and *b* values for MLO and several sets (covering different ranges of $m_w u$) for SGP conditions. For $S(\lambda)$ in (5) we used the filter function of the 941.4-nm channel as measured by the manufacturer (Barr Associates Inc., Westford, MA) in February 1994. The $V_o(\lambda)$ value of that channel was determined by averaging the results of 5 morning modified Langley plots (standard deviation 1.2%) performed at the Mauna Loa Observatory (MLO) two weeks before the IOP.

<u>Method B: Differential lamp/solar spectrum technique</u>

This method has been described in detail by Michalsky *et al.*[30] Only a brief summary is given here. Method B avoids the need to calibrate using the modified Langley method. Instead, it requires the instrument output $V_L(\lambda)$ when viewing a calibration lamp, the lamp irradiance $E_L(\lambda)$ and the extraterrestrial solar spectrum $E_0(\lambda)$, both convolved with the filter function $S(\lambda)$. In order to retrieve CWV we consider the ratio of the SPM output voltages measured in channels in (λ_{in}) and adjacent to (λ_{out}) the 0.94-μm band

$$\frac{V(\lambda_{in})}{V(\lambda_{out})} = \frac{E_0(\lambda_{in})E_L(\lambda_{out})V_L(\lambda_{in})}{E_0(\lambda_{out})E_L(\lambda_{in})V_L(\lambda_{out})} T_w(\bar{\lambda}) \exp\left[-m\left(\tau_R(\lambda_{in}) + \tau_a(\lambda_{in}) - \tau_R(\lambda_{out}) - \tau_a(\lambda_{out})\right)\right] \quad (9)$$

Solving for $T_w(\bar{\lambda})$ we can relate this calculated value to the radiative transfer model calculation of $T_w(\bar{\lambda})$ to derive CWV. It is important to note that in (9) most measurements and calculated values appear as relative values, which we can determine more accurately than absolute values.[23,31]

We have applied method B to the IOP data obtained from MFRSR and RSS. For MFRSR we used the 860-nm and 938-nm channels as λ_{out} and λ_{in}, respectively. $S(\lambda)$ of all MFRSR channels was measured in August 1996 and again in March 1998. The 938-nm channel shifted towards red by 0.8 nm, but no wavelength shift was observed for the other channels. In this paper we have used the August 1996 measurements of $S(\lambda)$. For RSS we used λ_{out} = 871 nm (pixel number 440) and λ_{in} = 943 nm (pixel number 458). The $S(\lambda)$ of each pixel has been established using lasers.[21] Because method B does not depend on modified Langley plots, no parametrization of $T_w(\bar{\lambda})$ is necessary, and $T_w(\bar{\lambda})$ can be converted into CWV using a look-up-table. For both instruments we used MODTRAN 3.7 v1.0 to create such a look-up-table of $T_w(\bar{\lambda})$ versus mu.

Method C: Empirical technique

In method C the signal in the 938-nm MFRSR-channel is calibrated for the retrieval of water vapor by estimating the adjusted signal, $V_w(\lambda)$ (the signal that would be measured if water vapor were the only attenuator) with the MFRSR while simultaneously observing the CWV, with another instrument nearby. The "other instrument" is a microwave radiometer (MWR) - the ARM CART (Cloud and radiation test bed) MWR measuring at *f*=31.4 and 23.8 GHz - that operates continuously at SGP.[32] An empirical curve can then be formed that shows the relationship between $V_w(\lambda)$ and mu. An equation fitted to this curve provides an algebraic

expression relating $V_w(\lambda)$ and mu so that if $V_w(\lambda)$ – the adjusted measurement – is known, then u can be found.

Using the definition of adjusted signal $V_w(\lambda)$ and equation (4), we have

$$V_w(\lambda) = V(\lambda)\exp\left[m\left(\tau_R(\lambda)+\tau_a(\lambda)+\tau_3(\lambda)\right)\right] = V_0(\lambda)R^{-2}T_w\left(\bar{\lambda}\right), \tag{10}$$

where $V(\lambda)$ is the measured voltage. $V_w(\lambda)$ is fitted by the four-parameter model shown below.

$$V_w(\lambda)R^2 = V_0(\lambda)\exp\left[-a(mu)^{b-\beta mu}\right] \tag{11}$$

The four parameters are $V_o(\lambda)$, a, b, and β, where $V_o(\lambda)$ is the calibration constant for the 938-nm channel and a, b, and β describe $T_w\left(\bar{\lambda}\right)$.

This form of $T_w\left(\bar{\lambda}\right)$ is similar to the less-complicated transmission function in (6). We tried the simpler form but it only worked over a small range of mu typical of dry conditions during the winter. To extend the applicability of the transmission function over a wider range of mu encompassing the entire variation in vapor over the course of a year, we were forced to add a path dependence term, $-\beta mu$, to the exponent b where β is a small correction term. With this addition the range of validity of (11) is about 28 cm $\geq$ mu $\geq$ 0 cm. Data from 15 days of clear sky conditions, spanning a period from 16 January to 28 August 1997 were used to determine $_o(\lambda)$ and to develop the empirical transmission function described above. These data consisted of 21278 20-second samples and the parameter values were found to be a=0.5411, b=0.5802, and β=0.003284 with u in units of precipitable centimeters.

In method C the need to calibrate using the modified Langley method and the use of a radiative transfer model are both avoided. However, we have to keep in mind that because the

parameters in (11) are determined by comparing to the MWR, method C cannot yield an independent measure of CWV.

4. Results

In the first round, as with the AOD intercomparison work,[17] we made no attempt to standardize on the use of the same radiative transfer model and its underlying water vapor spectroscopy (required for methods A and B). In the second round we used LBLRTM 5.10[33] for all method-A and -B retrievals. As with the AOD intercomparison work,[17] we compared all CWV retrievals to the AATS-6 results. Because of the different sampling strategies and days of operation, this resulted in as few as 466 to as many as ~19,000 samples in the comparisons. The results were analyzed in terms of time series (Figure 1 and Figure 2) and scatter plots (Figure 3 and Figure 4). Statistical summaries are given in table form in Table 2 and Table 3 and are visualized in Figure 5.

We found that the quality of the MFRSR retrievals (Methods B and C) deteriorates at larger slant-path water-vapor amounts, *mu*, prompting us to use MFRSR data with *mu*<23 cm. The Cimel and AATS-6 retrievals do not have that limitation and no RSS retrievals were available for large values of *mu.*

The scatter plots (Figure 3 and Figure 4) reveal a high correlation ($0.995 \leq r^2 \leq 0.999$) among the solar transmittance methods and a somewhat smaller correlation ($0.984 \leq r^2 \leq 0.986$) with the MWR. This is because the MWR and the optical instruments, despite their collocation did not observe the same volume of air as the viewing direction is zenith for MWR and slant path to sun for the SPMs and furthermore, the field-of-view of the MWR (4.5 and 5.9 (FWHM) at 31.4 and 23.8 GHz, respectively) is larger. Consequently, we observe that the small-scale variations in CWV are highly correlated among the sunphotometers whereas some of the small-

scale features are absent in the MWR data (Figure 2). Also, we generally find the correspondence between SPMs and MWR to be best around solar noon.

In the first round of comparison 3 different models have been used for the Method-A and -B retrievals. The results are shown in the left columns of Figure 3 and Figure 4, and are summarized in Table 2 and Figure 5. The differences between each method (including MWR) and AATS-6 range from 2.6% to 5.3% (rms). The mean differences are within ±0.1 cm and the mean ratios range from 0.97 to 1.03.

In the second round of comparison we used LBLRTM 5.10 (which includes the updated spectroscopy according to Giver *et al.*[12]) for all method-A and -B retrievals. Repeating the computation with LBLRTM 5.21 (the most recent version at the time of writing) led to identical results. In this second round we also deviated from the standard Cimel AERONET-CWV algorithm (which uses a typical 940-nm filter function for all instruments) by using the measured filter functions for the instruments #27 and #37. The results are shown in the right columns of Figure 3 and Figure 4 as scatter plots, and are summarized in Table 3 and Figure 5.

As seen from the time series in Figure 1 and Figure 2 the changes made in the second comparison had a significant effect. Overall they decreased the mean CWV by 8% for AATS-6 and by 13% for Cimel, RSS and MFRSR (method B). These decreases in CWV are consistent with the results reported by Ingold *et al.*[3] Although we observe an even better correlation among the different methods (r^2 closer to unity and smaller rms differences with respect to the best-fit line), we now find larger biases. The differences between each method (including MWR) and AATS-6 now range from 3.2% to 8.3% (rms). The mean absolute differences in CWV range from –0.22 to 0.16 cm with mean ratios between 0.92 and 1.06. The results of method A and B are now 6 to 14% lower than the results of the MWR and, consequently, of method C. When

compared to AATS-6, the MWR and MFRSR (method C) exhibit slopes deviating considerably from unity. Note that the MFRSR(method C) retrievals are tied to MWR results.

Even the spread among the results of the independent solar transmittance retrievals (methods A and B) has increased slightly. In terms of absolute differences (column 11 of Table 2 or Table 3) the spread is now 0.22 cm (0.19 cm before) or in terms of mean ratios (column 15 of Table 2 or Table 3) the spread increased from 6% to 8%. This shows that the result of the first comparison round was somewhat misleading because differences in the models obviously compensated for other existing biases. In other words, the remaining biases must be caused by errors other than model errors. For method A, those primarily include uncertainty in the calibration constant $V_o(\lambda)$, in the filter function $S(\lambda)$, in the parametrization of T_w and in aerosol optical depth $\tau_a(\lambda)$. A detailed analysis of these uncertainties can be found in Ingold *et al.*[3] For method B, uncertainties other than model errors include uncertainty in the filter function $S(\lambda)$, lamp irradiance ratio $E_L(\lambda_{in})/E_L(\lambda_{out})$, the relative extraterrestrial solar spectrum ratio $E_o(\lambda_{in})/E_o(\lambda_{out})$, and in $\tau_a(\lambda)$. A detailed discussion of these uncertainties is given by Michalsky et al. [2000]. In this work we have used the extraterrestrial solar spectrum compiled by Gueymard[34] for the method B retrievals. Using the spectrum of Kurucz[35] as contained in MODTRAN 3.7 increased the mean CWV by 1.3%.

5. Conclusion

We have in hand a large data set of CWV retrievals from four sunphotometers. We have used three different retrieval techniques and have also compared to a microwave radiometer (MWR) on which one of the techniques is based. The good agreement realized in the first round of comparison turns out to be fortuitous because differences in the radiative transfer models

obviously compensated for biases found once a single model was used for all independent retrievals. The spread of 0.22 cm or 8% among all independent SPM retrievals when using the same model is an indication of the other-than-model uncertainties involved in determining CWV from solar transmittance measurements with current instrumentation. These uncertainties include primarily uncertainties in calibration and filter or slit-function profile. The changes in H_2O spectroscopy suggested by Giver *et al.*[12] had a significant impact on the SPM retrievals: depending on which model was used initially they decreased the mean CWV by 8% or 13%. With the improved spectroscopy the CWV retrievals from the SPMs are now 6-14% lower than the MWR results. However, this result needs to be considered in context with all CWV measurements performed during the IOP. A publication showing all results from the 2nd Water Vapor IOP is in preparation.

Acknowledgements. The Office of Earth Science, NASA Headquarters (Robert Curran and Jack Kaye) and the NOAA Office of Global Programs (Joel Levy) funded this research in part (BAER, SRI, and NASA ARC). It was also supported by the Office of Biological and Environment Research of the U.S. Department of Energy as part of the Atmospheric Radiation Measurement Program.by grant DE-FG02-90ER61072 (SUNY) and by contract no. DE-AC02-98CH10886 (Brokhaven), CHENG82-1010502-0002884 (Ames) and W-31-109-Eng-38 (Argonne). Pacific Northwest National Laboratory is operated for the U.S. Department of Energy by Battelle Memorial Institute under contract DE-AC0676RLO 1830.The AERONET project is supported by the EOS Project Science Office (Michael King) and the Office of Earth Science, NASA Headquarters (Robert Curran).

References

1. F. E. Fowle, "The spectroscopic determination of aqueous vapor," Astrophys. J. **35**, 149-162 (1912).
2. R. M. Goody and Y. L. Yung, *Atmospheric Radiation*, Vol. 1, Theoretical Basis, 2nd ed., (Oxford University Press, NY, 1989).
3. T. Ingold, B. Schmid, C. Mätzler, P. Demoulin, and N. Kämpfer, "Modeled and Empirical Approaches for Retrieving Columnar Water Vapor from Solar Transmittance Measurements in the 0.72, 0.82 and 0.94-μm Absorption Bands," J. Geophys. Res. (submitted).
4. B. Schmid, J. M. Livingston, P. B. Russell, P. A. Durkee, H. H. Jonsson, D. R. Collins, R. C. Flagan, J. H. Seinfeld, S. Gassó, D. A. Hegg, E. Öström, K. J. Noone, E. J. Welton, K. J. Voss, H. R. Gordon, P. Formenti, and M. O. Andreae, "Clear sky closure studies of lower tropospheric aerosol and water vapor during ACE 2 using airborne sunphotometer, airborne in-situ, space-borne, and ground-based measurements," Tellus B **52**, 568-593 (2000).
5. W. P. Chu, E. W. Chiou, J. C. Larsen, L. W. Thomason, D. Rind, J. J. Buglia, S. Oltmans, M. P. McCormick, and L. M. McMaster, "Algorithms and Sensitivity Analyses for Stratospheric Aerosol and Gas Experiment II Water Vapor Retrieval", J. Geophys. Res. **98**, 4857-4866 (1993).
6. J. D. Lumpe, R. M. Bevilacqua, K. W. Hoppel, S. S. Krigman, D. L. Kriebel, C. E. Randall, D. W. Rusch, C. Brogniez, R. Ramananaherosa, E. P. Shettle, J. J. Olivero, J. Lenoble, and P. Pruvost, "POAM II Retrieval Algorithm and Error Analysis," J. Geophys. Res. **102**, 23'593–23'614 (1997).

7. B.-C. Gao, and A. F. H. Goetz, “Column atmospheric water vapor and vegetation liquid water retrievals from airborne imaging spectrometer data,” J. Geophys. Res. **95**, 3549–3564 (1990).

8. Y. J. Kaufman, and B.-C. Gao, “Remote Sensing of Water Vapor in the Near IR from EOS/MODIS,” IEEE Geosc. Rem. Sens. **30**, 871-884 (1992).

9. S. Bouffiès, F. M. Bréon, D. Tanré and P. Dubuisson, “Atmospheric water vapor estimate by a differential absorption technique with the polarisation and directionality of the Earth reflectances (POLDER) instrument,” J. Geophys. Res. **102**, 3831-3841 (1997).

10. M. Vesperini, F. M. Bréon, and D. Tanré, “Atmospheric water vapor content from spaceborne POLDER measurements,” IEEE Geosc. Rem. Sens. **37**, 1613-1619 (1999).

11. L. S. Rothman, C. P. Rinsland, A. Goldman, S. T. Massie, D. P. Edwards, J.-M. Flaud, A. Perrin, C. Camy-Peyret, V. Dana, J.-Y. Mandin, J. Schroeder, A. McCann, R. R. Gamache, R. B. Wattson, K. Yoshino, K. V. Chance, K. W. Jucks, L. R. Brown, V. Nemtchinov, and P. Varanasi, “The HITRAN Molecular Spectroscopic Database and HAWKS (HITRAN Atmospheric Workstation): 1996 Edition,” J. Quant. Spectr. Rad. Transf. **60**, 665-710 (1998).

12. L. P. Giver, C. Chackerian Jr., and P Varanasi, “Visible and near-infrared $H_2{}^{16}O$ line intensity corrections for HITRAN-96,” J. Quant. Spectr. Rad. Transf., **66**, 101-105 (2000).

13. R. C. M. Learner, W. Zhong, J. D. Haigh, D. Belmiloud, and J. Clarke, “The Contribution of Unknown Weak Water Vapor Lines to the Absorption of Solar Radiation,” Geophys. Res. Lett. **26**, 3609–3612 (1999).

14. M. Carleer, A. Jenouvrier, A.-C. Vandaele, P. F. Bernath, M. F. Mérienne, R. Colin, N. F. Zobov, O. L. Polyansky, J. Tennyson, and V. A. Savin, “The near infrared, visible, and near ultraviolet overtone spectrum of water,” J. Chem. Phys. **111**, 2444–2450 (1999).

15. G. M. Stokes and S. E. Schwartz, “The Atmospheric Radiation Measurement (ARM) program: Programmatic background and design of the cloud and radiation test bed,” Bull. Am. Meterol. Soc. **75**, 1201-1221 (1994).

16. H. E. Revercomb, W. F. Feltz, R. O. Knuteson, D. C. Tobin, P. F. W. van Delst, and B. A. Whitney, “Accomplishments of the Water Vapor IOPs: An Overview,” Proceedings of the Eighth Atmospheric Radiation Measurement (ARM) Science Team Meeting March 23-27, 1998, Tucson, Arizona.

17. B. Schmid, J. Michalsky, R. Halthore, M. Beauharnois, L. Harrison, J. Livingston, P. Russell, B. Holben, T. Eck, and A. Smirnov, “Comparison of Aerosol Optical Depth from Four Solar Radiometers During the Fall 1997 ARM Intensive Observation Period,” Geophys. Res. Lett. **26**, 2725-2728 (1999).

18. T. Matsumoto, P. B. Russell, C. Mina, W. Van Ark and V. Banta, “Airborne Tracking Sunphotometer,” J. Atmos. Ocean. Tech. **4**, 336-339 (1987).

19. B. N. Holben, T. F. Eck, I. Slutsker, D. Tanré, J. P Buis, A. Setzer, E. Vermote, J. A. Reagan, Y. J. Kaufman, T. Nakajima, F. Lavenu, I. Jankowiak, and A. Smirnov, “AERONET: a federated instrument network and data archive for aerosol characterization,” Remote Sens. Environ. **66**, 1-16 (1998).

20. L. Harrison J. Michalsky, and J. Berndt, “Automated multifilter rotating shadow-band radiometer: an instrument for optical depth and radiation measurements,” Appl. Opt. **33**, 5118-5125 (1994).

21. Harrison, L., M. Beauharnois, J. Berndt, P. Kiedron, J.J. Michalsky, and Q. Min, “The Rotating Shadowband Spectroradiometer (RSS) at SGP,” Geophys. Res. Lett. **26**, 1715-1718 (1999).

22. B. Schmid and C. Wehrli, “Comparison of Sun Photometer Calibration by Langley Technique and Standard Lamp,” Appl. Opt. **34**, 21, 4500-4512 (1995).

23. B. Schmid, P. R. Spyak, S. F. Biggar, C. Wehrli, J. Sekler, T. Ingold, C. Mätzler, and N. Kämpfer, “Evaluation of the applicability of solar and lamp radiometric calibrations of a precision Sun photometer operating between 300 and 1025 nm,” Appl. Opt. **37**, 3923-3941 (1998).

24. P. B. Russell, J. M. Livingston, E. G. Dutton, R. F. Puschel, J. A. Reagan, T. E. Defoor, M. A. Box, D. Allen, P. Pilewski, B. M. Herman, S. A. Kinne, and D. J. Hofmann, “Pinatubo and Pre-Pinatubo Optical-Depth Spectra: Mauna Loa Measurements, Comparisons, Inferred Particle Size Distributions, Radiative Effects, and Relationship to Lidar Data,” J. Geophys. Res. **98**, 22,969-22,985 (1993).

25. J. A. Reagan, P. A. Pilewskie, I. C. Scott-Fleming, B. M. Herman and A. Ben-David, “Extrapolation of Earth-Based Solar Irradiance Measurements to Exoatmospheric Levels for Broad-Band and Selected Absorption-Band Observations’” IEEE Geosc. Rem. Sens. **25**, 647-653 (1987).

26. J. J. Michalsky. J. C. Liljegren, and L. C. Harrison, “A comparison of Sun photometer derivations of total column water vapor and ozone to standard measures of same at the Southern Great Plains Atmospheric Radiation Measurement site,” J. Geophys. Res. **100**, 25,995-26,003 (1995).

27. B. Schmid, K. J. Thome, P. Demoulin, R. Peter, C. Mätzler, and J. Sekler, “Comparison of Modeled and Empirical Approaches for Retrieving Columnar Water Vapor from Solar Transmittance Measurements in the 0.94 Micron Region,” J. Geophys. Res. **101**, 9345-9358, (1996).

28. R. N Halthore, T. F. Eck, B. N. Holben and B. L. Markham, “Sun photometric measurements of atmospheric water vapor column abundance in the 940-nm band,” J. Geophys. Res., **102**, 4343-4352 (1997).

29. F. X. Kneizys, L. W. Abreu, G. P. Anderson, J. H. Chetwynd, E. P. Shettle, A. Berk, L. S. Bernstein, D. C. Robertson, P. Acharaya, L. S. Rothmann, J. E. A. Selby, W. O. Gallery, and S. A. Clough, “The Modtran 2/3 Report and LOWTRAN 7 Model”, 11. Jan. 1996, Phillips Laboratory, Geophysics Directorate PL/GPOS, 29 Randolph Road, Hanscom AFB, MA 01731-3010.

30. J. J. Michalsky, Q. Min, P. W. Kiedron, D. W. Slater, and J. C. Barnard, “A differential technique to retrieve column water vapor using sun radiometry,” J. Geophys. Res. (in press).

31. P. W. Kiedron, J. J. Michalsky, J. L., Berndt and L. C. Harrison, “Comparison of spectral irradiance standards used to calibrate shortwave radiometers and spectroradiometers,” Appl. Opt. **38**, 2432-2439 (1999).

32. J. C. Liljegren, “Automatic self-calibration of ARM microwave radiometers,” in Microwave Radiometry and Remote Sensing of the Earth's Surface and Atmosphere, P. Pampaloni and S. Paloscia (eds.), (VSP Press, Utrecht, 1999).

33. S. A. Clough, and M. J. Iacono, “Line-by-Line Calculations of Atmospheric Fluxes and Cooling Rates II: Application to Carbon Dioxide, Ozone, Methane, Nitrous Oxide, and the Halocarbons,” J. Geophys. Res. **100**, 16,519-16,535 (1995).

34. C. Gueymard, “SMARTS2, a simple model of the atmospheric radiative transfer of sunshine: Algorithms and performance assessment,” FSEC-PF-270-95, Florida Solar Energy Center, Cocoa, Florida (1995).

35. R. L. Kurucz, “The solar irradiance by computation,” *Proceedings of the 17th Annual Conference on Atmospheric Transmission Models*, 8-9 June 1994. Phillips Laboratory Directorate of Geophysics, Hanscom, AFB, MA 01731-3010, Editors: G.P. Anderson, R.H. Picard, J.H. Chetwind, 24 May 1995, PL-TR-95-2060, pp. 333-334.

Figure 1: Time series of columnar water vapor from different instruments and methods. Top: initial comparison where no attempts have been made to standardize on one radiative transfer model. Bottom: All method-A and –B retrievals use the same radiative transfer model (LBLRTM 5.10).

Figure 2: Same as Figure 1 but shown are only two hours to better see small-scale variations.

Figure 3: CWV intercomparison with respect to AATS-6. Left column: initial comparison where no attempts have been made to standardize on one radiative transfer model. Right column: All retrievals done using the same radiative transfer model (LBLRTM 5.10).

Figure 4: CWV intercomparison with respect to AATS-6. Left column: initial MODTRAN 3.5 was used for AATS-6. Right column: LBLRTM 5.10 was used for AATS-6.

Figure 5: Statistics for CWV intercomparison with respect to AATS-6. Top: initial comparison where no attempts have been made to standardize on one radiative transfer model. Right column: All method-A and –B retrievals use the same radiative transfer model (LBLRTM 5.10).

Table 1: Central Wavelengths (λ) and Bandwidths (Δλ, Full Widths at Half Maximum) of Filtered Instruments.

AATS-6		CIMEL		MFRSR	
λ[nm]	Δλ [nm]	λ [nm]	Δλ [nm]	λ [nm]	Δλ [nm]
		340	2		
380.1	5.0	380	4		
				413.9	10
450.7	5.1	440	10		
525.3	5.0	500	10	499.3	10
				608.5	10
		670	10	665.1	10
863.9	5.3	870	10	859.9	10
941.4	5.8	940	10	938.0	10
1020.7	5.0	1020	10		

Table 2: Comparison of CWV from different instruments and methods to AATS-6. This is the initial comparison where different radiative transfer models as indicated have been used.

Instrument	Method	Model		Best Fit				Mean (cm)		Differences (cm)				Ratios y/AATS-6	
			n	slope	inter (cm)	r^2	RMS (cm)	AATS-6	y	mean	stdev	RMS	RMS(%)	mean	stdev
AATS-6	A	MODTRAN 3.5													
Cimel	A	LOWTRAN 7	466	1.05	-0.03	0.997	0.06	2.83	2.93	0.10	0.08	0.13	4.4%	1.03	0.02
RSS	B	MODTRAN 3.7	4015	0.98	-0.01	0.995	0.07	3.06	2.98	-0.09	0.07	0.11	3.7%	0.97	0.02
MFRSR	B	MODTRAN 3.7	14649	1.01	0.03	0.996	0.06	2.73	2.77	0.04	0.06	0.07	2.6%	1.02	0.02
MFRSR	C	n/a	18957	0.98	-0.01	0.997	0.05	2.86	2.78	-0.08	0.06	0.10	3.4%	0.97	0.02
MWR CART	n/a	n/a	16990	1.00	-0.09	0.984	0.12	2.87	2.79	-0.09	0.12	0.15	5.3%	0.97	0.05

Table 3: Same as Table 2 but the same radiative transfer model has been used for all method-A and –B retrievals.

Instrument	Method	Model		Best Fit				Mean (cm)		Differences (cm)				Ratios y/AATS-6	
			n	slope	inter (cm)	r^2	RMS (cm)	AATS-6	y	mean	stdev	RMS	RMS(%)	mean	stdev
AATS-6	A	LBLRTM 5.10													
Cimel	A	LBLRTM 5.10	466	0.99	-0.03	0.997	0.05	2.60	2.54	-0.06	0.05	0.08	3.2%	0.97	0.02
RSS	B	LBLRTM 5.10	4022	0.95	-0.08	0.998	0.04	2.80	2.59	-0.22	0.06	0.22	8.0%	0.92	0.02
MFRSR	B	LBLRTM 5.10	14703	0.97	-0.02	0.998	0.03	2.50	2.41	-0.10	0.04	0.10	4.1%	0.96	0.01
MFRSR	C	n/a	18996	1.09	-0.07	0.999	0.04	2.63	2.78	0.16	0.09	0.18	6.9%	1.06	0.02
MWR CART	n/a	n/a	17145	1.12	-0.15	0.986	0.12	2.64	2.79	0.15	0.16	0.22	8.3%	1.05	0.05

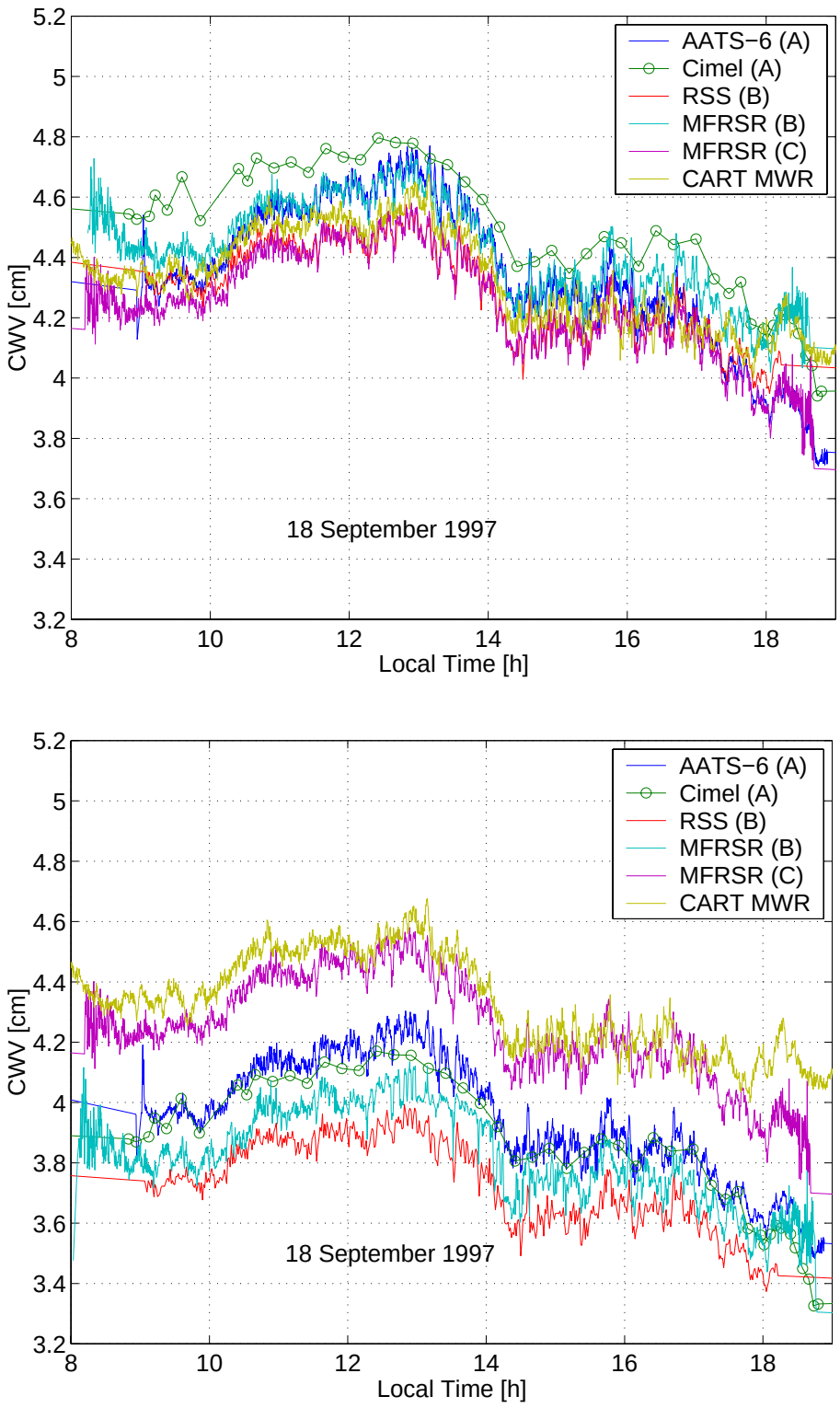
AATS−6 (A)
Cimel (A)
RSS (B)
MFRSR (B)
MFRSR (C)
CART MWR
CWV [cm]
Local Time [h]
18 September 1997
5.2
5
4.8
4.6
4.4
4.2
4
3.8
3.6
3.4
3.2
8
10
12
14
16
18

Figure 1

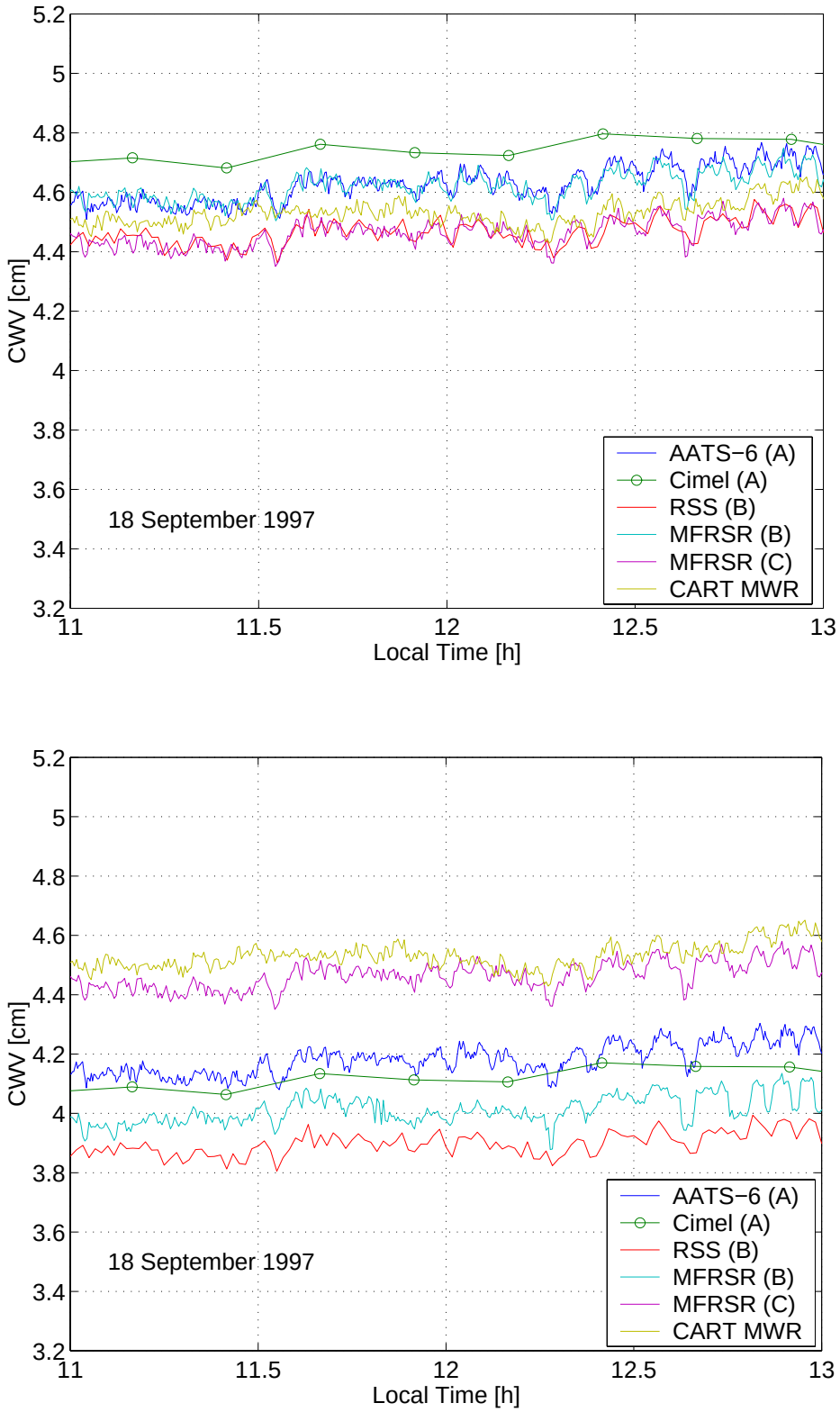
5.2
5
4.8
4.6
4.4
4.2
4
3.8
3.6
3.4
3.2
CWV [cm]
11
11.5
12
12.5
13
Local Time [h]
18 September 1997
AATS−6 (A)
Cimel (A)
RSS (B)
MFRSR (B)
MFRSR (C)
CART MWR
5.2
5
4.8
4.6
4.4
4.2
4
3.8
3.6
3.4
3.2
CWV [cm]
11
11.5
12
12.5
13
Local Time [h]
18 September 1997
AATS−6 (A)
Cimel (A)
RSS (B)
MFRSR (B)
MFRSR (C)
CART MWR

Figure 2

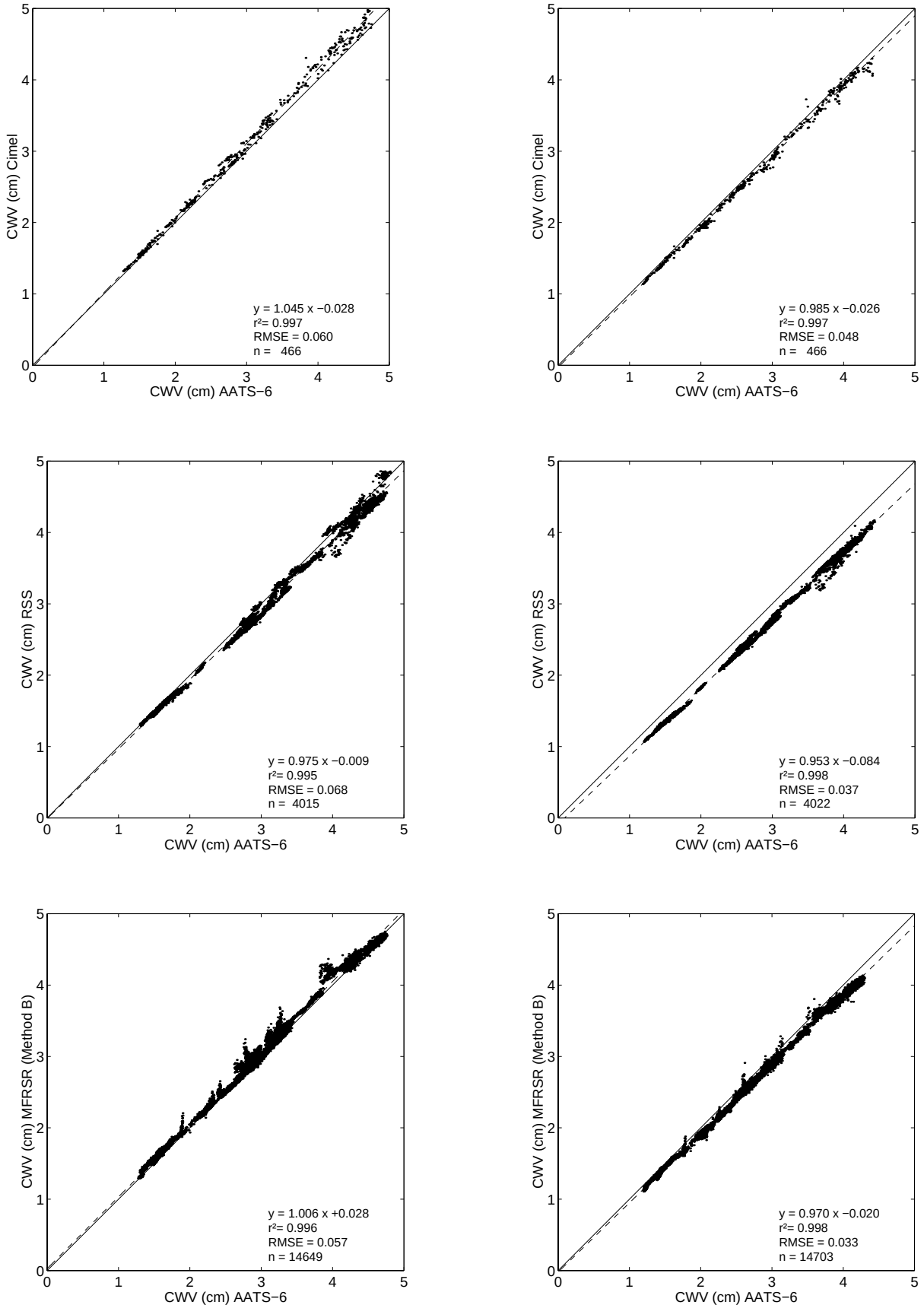
CWV (cm) Cimel
CWV (cm) AATS−6
y = 1.045 x −0.028
r²= 0.997
RMSE = 0.060
n = 466
CWV (cm) Cimel
CWV (cm) AATS−6
y = 0.985 x −0.026
r²= 0.997
RMSE = 0.048
n = 466
CWV (cm) RSS
CWV (cm) AATS−6
y = 0.975 x −0.009
r²= 0.995
RMSE = 0.068
n = 4015
CWV (cm) RSS
CWV (cm) AATS−6
y = 0.953 x −0.084
r²= 0.998
RMSE = 0.037
n = 4022
CWV (cm) MFRSR (Method B)
CWV (cm) AATS−6
y = 1.006 x +0.028
r²= 0.996
RMSE = 0.057
n = 14649
CWV (cm) MFRSR (Method B)
CWV (cm) AATS−6
y = 0.970 x −0.020
r²= 0.998
RMSE = 0.033
n = 14703

Figure 3

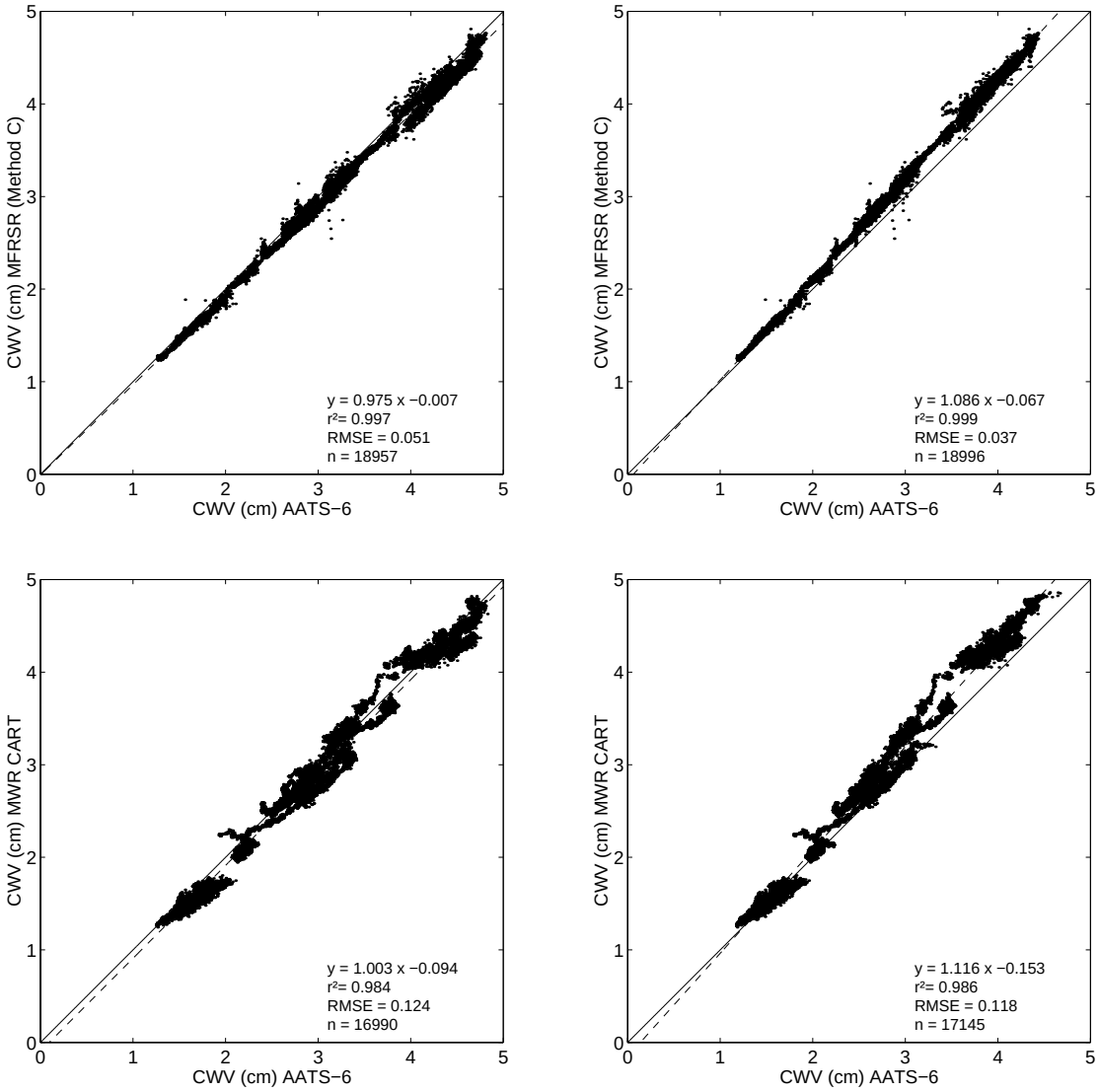
CWV (cm) MFRSR (Method C)
CWV (cm) AATS−6
y = 0.975 x −0.007
r²= 0.997
RMSE = 0.051
n = 18957
CWV (cm) MFRSR (Method C)
CWV (cm) AATS−6
y = 1.086 x −0.067
r²= 0.999
RMSE = 0.037
n = 18996
CWV (cm) MWR CART
CWV (cm) AATS−6
y = 1.003 x −0.094
r²= 0.984
RMSE = 0.124
n = 16990
CWV (cm) MWR CART
CWV (cm) AATS−6
y = 1.116 x −0.153
r²= 0.986
RMSE = 0.118
n = 17145

Figure 4

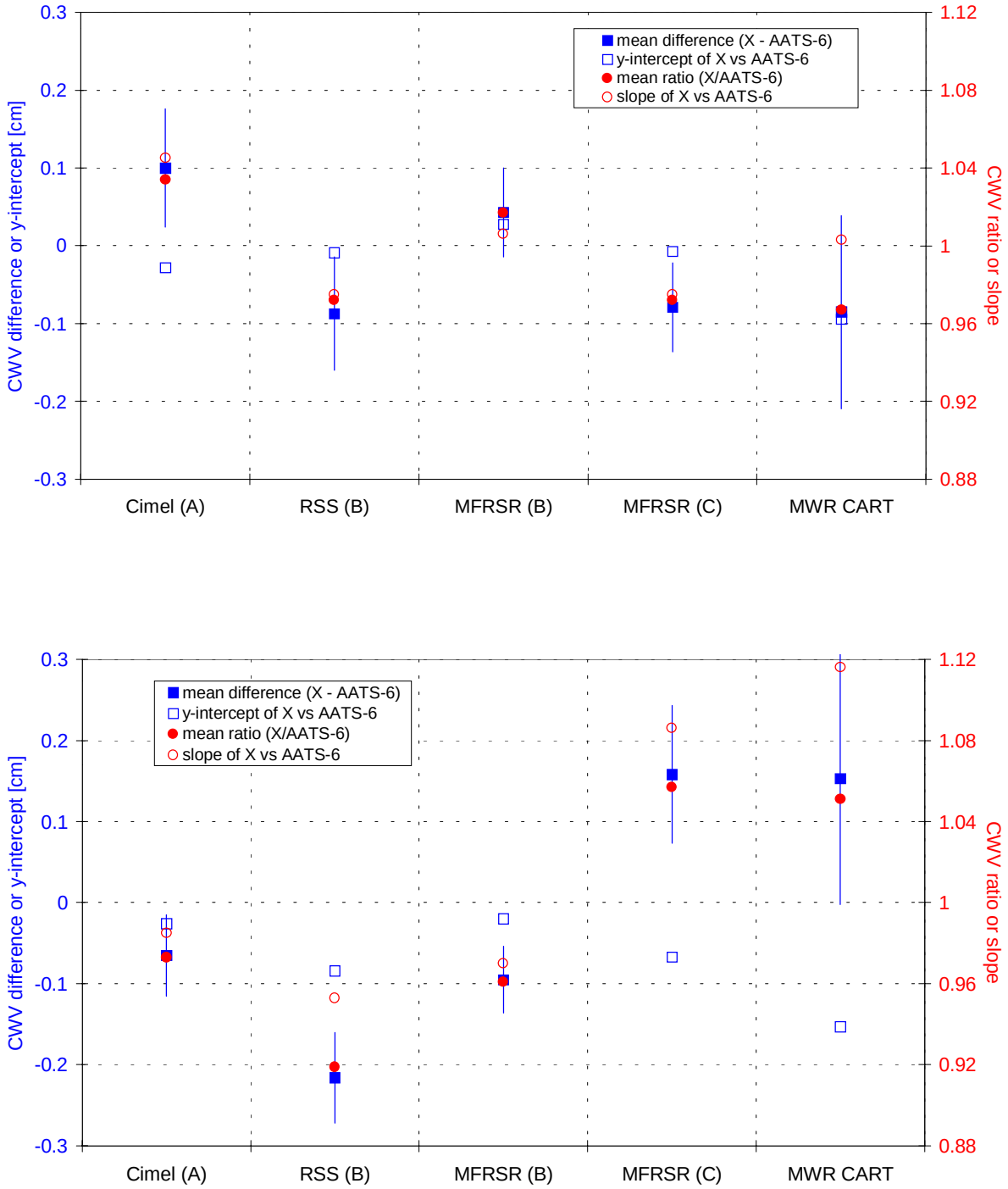
mean difference (X - AATS-6)
y-intercept of X vs AATS-6
mean ratio (X/AATS-6)
slope of X vs AATS-6
CWV difference or y-intercept [cm]
CWV ratio or slope
0.3
0.2
0.1
0
-0.1
-0.2
-0.3
1.12
1.08
1.04
1
0.96
0.92
0.88
Cimel (A)
RSS (B)
MFRSR (B)
MFRSR (C)
MWR CART
mean difference (X - AATS-6)
y-intercept of X vs AATS-6
mean ratio (X/AATS-6)
slope of X vs AATS-6
CWV difference or y-intercept [cm]
CWV ratio or slope
0.3
0.2
0.1
0
-0.1
-0.2
-0.3
1.12
1.08
1.04
1
0.96
0.92
0.88
Cimel (A)
RSS (B)
MFRSR (B)
MFRSR (C)
MWR CART

Figure 5